Long *et al. Geoscience Letters* (2025) 12:10
https://doi.org/10.1186/s40562-025-00383-9

Geoscience Letters

RESEARCH LETTER

Open Access

Enhanced seasonal contrast of surface mixed layer depth in the North Indian Ocean under a CO_2 removal scenario

Shang-Min Long[1,2,3*], Chenyi Sun[1,2], Zhen Gao[4,5], Ming Feng[3], Xia Qu[6,7], Gang Huang[7,8,9] and Xingrong Chen[2,10]

Abstract

The surface mixed layer depth (MLD) of the tropical Indian Ocean is projected to shoal significantly under increased atmospheric CO_2, but its further response to subsequent CO_2 removal remains unclear. This work investigates this issue utilizing climate models' simulations under an idealized scenario with symmetric increase and decrease in atmospheric CO_2. The results show that the increased CO_2-induced basin-wide MLD shoaling recovers rapidly when CO_2 decreases. However, the MLD changes display large spatial variations and leave a prominent overall deepening trend in the North Indian Ocean (NIO) but an overall shoaling trend south of 10°S when CO_2 returns to its initial level. The former comprises an overall deepened winter deep MLD but shoaled summer MLD, amplifying the seasonal MLD contrast north of 10°N. The overall winter deepening is dominated by a prominent Newtonian cooling over large residual surface warming as the overall winter monsoon changes are weak when CO_2 level is restored. While the overall summer shoaling primarily results from the prominent monsoon weakening, the shoaling effect from reduced wind overwhelm the Newtonian cooling by reducing wind stirring, suppressing latent heat loss and increasing cloud-related radiative flux. In contrast, the overall MLD shoaling south of 10°S displays minor seasonal differences due to persistent weakening in the trade winds year-round, resulting from an enhanced Southern Ocean warming. Despite complicated ocean–atmosphere coupling processes in the overall Indian Ocean MLD trend, the residual sea surface warming and distinct winter and summer changes are essential. The results highlight the compound and coupled effects of different surface forcing on MLD changes under external forcing and imply that while CO_2 removal actions can largely recover the Indian Ocean MLD shoaling and seasonal cycle changes induced by anthropogenic warming, nonlinear atmospheric response may leave asymmetric changes in oceanic conditions and hence climatic and biological systems.

Keywords Indian Ocean, Mixed layer depth, Climate change, Carbon dioxide removal, Seasonal cycle, Ocean–atmosphere coupling

*Correspondence:
Shang-Min Long
smlong@hhu.edu.cn
Full list of author information is available at the end of the article

Introduction

The surface ocean mixed layer (ML) plays a critical role in the ocean environment, serving as a dynamic interface associated with complicated physical, chemical and biological processes. The ML depth (MLD) significantly evolves over time and regions and is an essential metric of the ocean environment. Particularly, seasonal deepening of the MLD promotes nutrient entrainment from subsurface waters, supporting phytoplankton blooms and promoting the formation of water mass. Therefore, MLD variations are also fundamental for understanding changes in regional climate (Shi et al. 2024; Liu et al. 2024a), marine heatwaves (Amaya et al. 2021; Elzahaby et al. 2022; Shi et al. 2022), and ecosystems (Fu et al. 2016; Breitburg et al. 2018; Cai et al. 2020).

Under global warming, the ML responds rapidly to external forcing and is closely linked to changes in absorption and storage of anthropogenic heat and carbon (Liu et al. 2018; Bourgeois et al. 2022; Li et al. 2023). The MLD is determined by mechanical (wind) stirring, buoyancy forcing (heat and freshwater), and ocean dynamical (advection) effects (Liu and Lu 2016; Somavilla et al. 2017). The MLD under global climate change are supposed to shoal under enhanced upper ocean warming over most oceans (Li et al. 2020; Peng and Wang 2024). However, due to different drivers such as surface warming/cooling and freshening/salinizing, decreased/increased wind speed and upper-ocean thermal and dynamical adjustments (Sallée et al. 2021; Long et al. 2024), MLD may shoal over specific regions and deepen or display insignificant changes in other regions. Indeed, the global ocean's vertical stratification strengthened by 7–8%, accompanied by a 4 m deepening of the MLD (Roch et al. 2023) during 2006–2021 despite upper ocean stratification increases (Li et al. 2020).

The dominant drivers of MLD changes also vary across regions. During 1960–2004, the deepening of winter MLD in the North Atlantic is linked to changes in wind stress and buoyancy forcing, whereas the shoaling trend in the Pacific MLD is likely due to the upper-ocean warming (Carton et al. 2008). In the Southern Ocean (SO), the strengthening of the westerlies is more pronounced in summer than winter during recent decades and lead to a MLD deepening in summer and shoaling in winter (Zhang et al. 2024a). The weakened seasonal cycle of MLD in the South Indian Ocean is determined by both the background oceanic conditions and a poleward shift of the trade winds (Long et al. 2024). In future warming scenarios, ocean absorbs more heat and stratification strengthens further, which favors MLD shoaling (Yeh et al. 2009; Somavilla et al. 2017) that is suggested to be generally larger during local winter and summer in the North Pacific (Chen and Wang 2015) and Indian Ocean (Gao et al. 2023). Under future low- and high-emission scenarios, the tropical Indian Ocean (TIO) MLD shoaling is dominated by surface net heat increase in the North Indian Ocean (NIO) and the joint effect of surface heat flux and wind changes in the South Indian Ocean (Gao et al. 2023). MLD changes exhibit substantial regional and seasonal differences under global climate change and require further studies in associated seasonal cycle changes and underlying mechanisms.

The continuous increase in atmospheric CO_2 concentrations since the Industrial Revolution has caused widespread severe impacts on global climate and ecological systems (Cheng et al. 2025). Achieving the 1.5 °C and 2 °C low-warming goal proposed by the 2015 Paris Agreement requires ambitious efforts toward the carbon–neutral target and even carbon dioxide removal (CDR) actions (Field and Mach 2017; Sanderson et al. 2017). The climate response under CDR scenarios is of great significance for society (Wu et al. 2010) and thus is designed to explore in the Coupled Model Intercomparison Project phase 6 (CMIP6, Eyring et al. 2016). Previous studies suggest that CDR actions cannot ensure full recovery of the regional climate change caused by the antecedent atmospheric CO_2 increase (Zhou et al. 2022; Zhang et al. 2023, 2024a, b). However, the seasonal cycle change of MLD and associated underlying processes under CDR scenarios are still poorly understood in the TIO.

Therefore, the present study investigates the TIO MLD response to an idealized CO_2 forcing scenario, in which CO_2 first increases and then symmetrically decreases, utilizing outputs from the CMIP6 and its subordinate CDR Model Intercomparison Project (CDRMIP, Keller et al. 2018). The rest of the present study is organized as follows. Sect. "Data and methods" describes the data and method. Sect. "Results" presents the results. Sect. "Summary and discussion" is a summary with discussion.

Data and methods

Data

The present study examines the performance of models in reproducing the TIO MLD by historical simulations and BOA-Argo data (Li et al. 2017). Then outputs of two idealized experiments, *1pctCO2* and *1pctCO2-cdr*, from 9 climate models (Table S1) are analyzed. In the *1pctCO2* experiment, the atmospheric CO_2 concentrations increase at a rate of 1%/year from the preindustrial level to quadruple level at year 140. Then the atmospheric CO_2 concentrations decrease at a rate of 1%/year from the quadruple level to the preindustrial level in *1pctCO2*

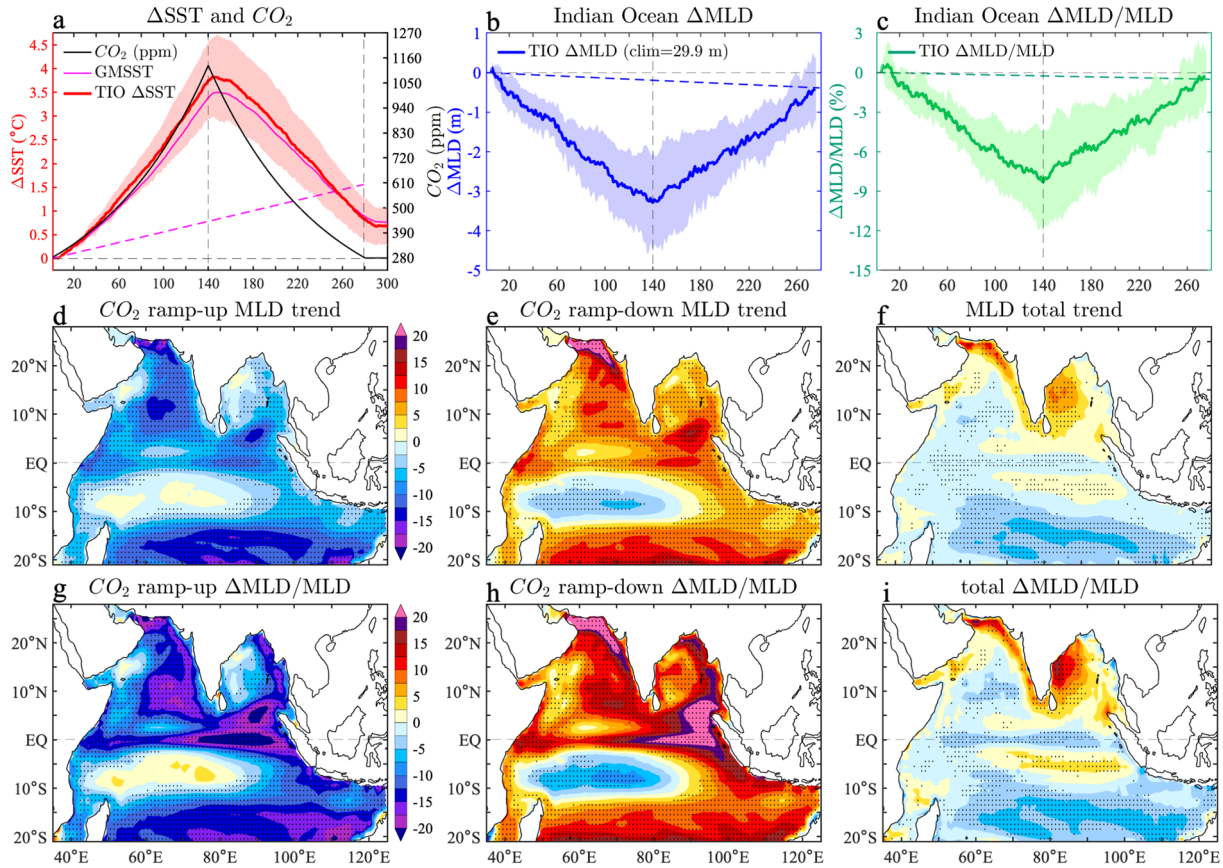

Fig. 1 Temporal evolution of annual–mean (**a**) atmospheric CO_2 concentration (ppm, black line) and multi-model ensemble–mean global–mean SST (GMSST, °C, magenta line) and tropical Indian Ocean–mean SST (TIO SST, red line) in 1pctCO2 and 1pctCO2-cdr experiments, with a 9-year running mean and a linear fit (dashed lines) being applied; (**b**) TIO–mean MLD change (Δ*MLD*, m) and (**c**) MLD percentage change (Δ*MLD*/*MLD*, %). The linear trend pattern of MLD during (**d**) years 1–140 (ramp-up period) and (**e**) years 140–279 (ramp-down period) and (**f**) years 1–279 (the whole period). The dots indicate regions with at least 75% of the models agreeing on the sign of the MME change. Panels (**g–i**) are the same as (**d–f**) but for percentage MLD changes (Δ*MLD*/*MLD*, %)

experiment (Fig. 1, black line). The two experiments provide a consecutive 279-year simulation with symmetric CO_2 increase and decrease. The years 1–140 and 140–279 are, respectively, defined as CO_2 ramp-up and ramp-down periods. Only one member of each model is utilized, and all variables are interpolated into a common grid for multi-model ensemble–mean (MME) analyses.

Methods

The MLD is directly available as 'mlotst' in most CMIP models (Table S1). For models without 'mlotst' output, we calculated the MLD as the depth at which the seawater potential density exceeding its surface value at a criterion of $\delta\rho = 0.125\ \mathrm{kg/m^3}$. Indeed, the MLD calculated based on this criterion is close to the direct MLD product from BOA-Argo, which defines the MLD by the objective maximum angle method (Chu and Fan. 2021).

The model-simulated TIO MLD is consistent with the Argo result in spatial pattern (Fig. S1) in climatology (2004–2014), with deep MLD in the Arabian Sea and South Indian Ocean and shallow MLD within 10°S–10°N and the Bay of Bengal. The MLD is generally underestimated in most models (Table S1) mainly due to underestimated winds (Pang et al. 2024) and coupled sea surface temperature (SST) biases (Gao et al. 2024). The MME climatology MLD (Fig. S1i) performs better than most models in reproducing the Argo results.

The ML mass conservation equation below (Jacob et al. 2000) is applied to examine different factors influencing the MLD change, which includes the ocean horizontal mass advection, vertical motion, entrainment effect from surface wind stress (τ), surface net heat flux (Q_{net}) and freshwater flux (W_{net}), and residual term induced by other processes:

$$\frac{\partial h}{\partial t} = -\vec{u} \cdot \nabla h - w_{-h} + \text{Entrainment} + \text{residual} \quad (1)$$

where h is MLD, $\overrightarrow{u}$ the horizontal currents, w_{-h} the vertical velocity at the ML bottom and is estimated as Ekman pumping velocity $W_{ek} = curl(\overrightarrow{\tau}/f)$ as vertical velocity is not available in some models.

The relative contributions of Q_{net} andW_{net}, both positive downward, on the MLD changes can be estimated by calculating the thermal $\left(BuoyT = \frac{\alpha g Q_{net}}{\rho_0 C_p}\right)$ and saline $\left(BuoyS = \frac{\beta S_0 g W_{net}}{\rho_0}\right)$ components of surface buoyancy flux, where S_0 is the sea surface salinity, and $\rho_0 = 1025\,\text{kg/m}^3$ is the seawater density. The specific heat capacity of seawater $C_p = 3980\text{J}\left(\text{kg}^{\circ}C\right)^{-1}$, α and β are, respectively, the thermal expansion and saline contraction coefficients. Positive changes in surface buoyance andW_{ek}, respectively, indicate shoaling effect on MLD, we thus use $-BuoyT$, $-BuoyS$ and $-W_{ek}$ to shift their signs consistent with the sign of MLD change for easy comparison.

Moreover, the surface latent heat (Q_e) of the Q_{net} can further be decomposed into a oceanic component $Q_e^o = \alpha_t \overline{Q_e} T'$, where $\alpha_t = L/R_v T^2$, L is latent heat of evaporation, R_v is the gas constant for water vapor, $\overline{Q_e}$ is climatology latent heat flux, and $T\prime$ and T are the change and climatology of SST) and an atmospheric component ($Q_e^a = Q_e - Q_e^o$) based on Taylor expansion, which are quite influential in ML heat budget (Xie et al. 2010). The wind speed effect ($Q_e^w = \overline{Q_e} \cdot W'/\overline{W}$, where $W\prime$ and $\overline{W}$ are receptively the change and climatology of wind speed) is an important subcomponent of Q_e^a and the estimation of the wind–evaporation–SST (WES) feedback (Xie and Philander 1994).

Results

Annual–mean MLD responses to CO_2 increase and decrease

During the CO_2 ramp-up period, the MME area–mean SST of the global ocean (GMSST) and TIO both increase rapidly (Fig. 1a). After year 140, the GMSST continues to increase for about 5 years due to delayed ocean slow response (Held et al. 2010; Long et al. 2014) and then gradually decreases. However, a prominent residual warming trend remains when atmospheric CO_2 is restored to the preindustrial level. The temporal evolution of the TIO SST mimics the GMSST trajectory and displays a similar magnitude of residual warming. This suggests prominent asymmetric response of global ocean and regional SST to a symmetric atmospheric CO_2 increase and subsequent decrease.

The MME basin–mean TIO MLD shoals when atmospheric CO_2 increases and rapidly recovers when CO_2 decreases (Fig. 1b), without a noticeable delay relative to the CO_2 peak. When CO_2 is restored, the overall MME MLD change tends to be slight shoaling. The MLD changes calculated by different density criteria from 0.03 to 0.125 kg/m^3 are highly similar (Fig. S2), suggesting that the results are not sensitive to the variations in the criterion.

However, the linear trends of MLD during different periods display substantial spatial variations (Fig. 1d–f). During the CO_2 ramp-up period, significant MLD shoaling trends occur over broad regions, especially over the Arabian Sea and south of 10°S, while weak shoaling or even slight deepening trends appear over the south equatorial thermocline dome, where model consistency is substantially low (Fig. 1d). The MLD shoaling is also evident on the equator, especially in the western and eastern parts, mainly due to equatorial wind changes and associated ocean–atmosphere coupling (Xie et al. 2010; Chadwick et al. 2013; Liu et al. 2015) through the WES feedback (Xie and Philander 1994) and Bjerknes feedback (Bjerknes 1969). These features are similar in the result based on 28 CMIP6 models (Fig. S4). In contrast, the TIO MLD trend during the CO_2 ramp-down period displays a nearly opposite pattern, with prominent deepening in the Arabian Sea, eastern Indian Ocean and south of 10°S. The thermocline dome region still displays weak trends (Fig. 1e). Indeed, the spatial correlation coefficient between the MLD trend patterns during ramp-up and ramp-down periods is as high as −0.85, suggesting an efficient recovery of MLD by CDR actions. However, the overall MLD trend during the whole period (years 1–279) displays a prominent deepening in the NIO, especially around the Indian Subcontinent, while a shoaling south of 10°S. The opposing changes across regions largely offset each other, resulting in a weak overall change in basin–mean MLD. In other regions, the overall MLD trend is negligible. Given the inter-model differences in the climatological MLD, the MME of the percentage changes in MLD relative to each model's climatology is further estimated (Fig. 1c, g–i). The percentage changes display similar temporal evolutions and spatial patterns with those of the raw changes, with MLD shoaling and deepening over specific regions exceeding 20% of the climatological value during ramp-up and ramp-down periods, respectively. Moreover, the overall MLD deepening in the NIO (~ 10%) and shoaling south of 10°S (5%) further highlight a prominent north–south differences in MLD response to symmetric CO_2 forcing. The overall MLD deepening in the NIO and shoaling south of 10°S is

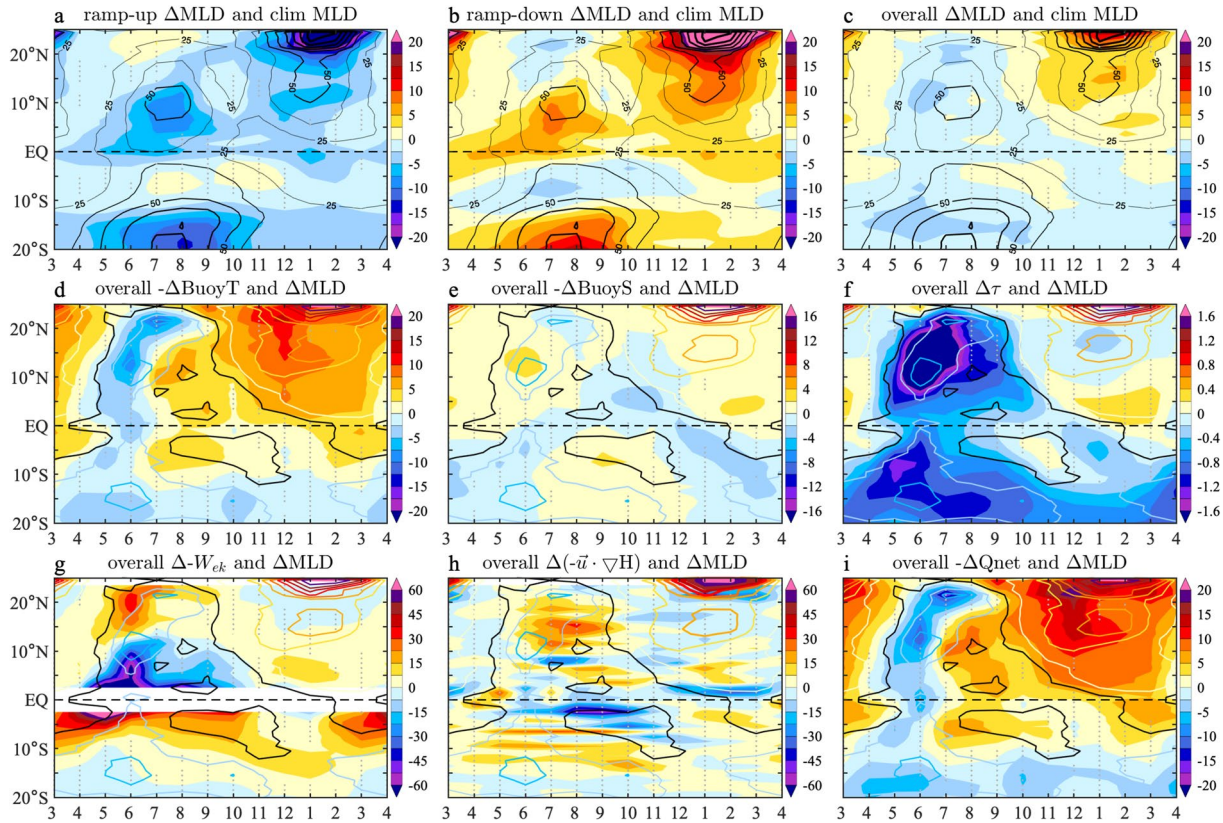

Fig. 2 Seasonal evolution of the zonal–mean (50–100°E) MLD in climatology (contours) and linear trends during (**a**) ramp-up period, (**b**) ramp-down period and (**c**) the whole period (overall trend). In addition, the zonal–mean of overall trends in surface buoyance flux change induced by (**d**) surface heat flux change ($-\Delta BuoyT$) and (**e**) freshwater flux change ($-\Delta BuoyS$), and in (**f**) wind stress ($\Delta\tau$, N/m^2), (**g**) Ekman pumping ($-\Delta W_{ek}$, positive downward), (**h**) horizontal mass advection ($-\overrightarrow{u}\cdot\nabla h$) and (**i**) net surface heat flux ($-\Delta Q_{net}$, positive upward). The dots indicate at least 75% models agreeing on the sign of the change, and the contours in panels (**d–i**) is the overall trends in MLD, with zero contour in thick black

also evident in most models despite differences in magnitude (Fig. S3).

Seasonal evolution of the MLD responses

Surface buoyancy and wind forcing are two dominant factors influencing the TIO MLD changes (Gao et al. 2023; Long et al. 2024), both of which display substantial seasonality in the Indian Ocean, where monsoon dynamics and intense ocean–atmosphere interaction primarily shape the climate. Consequently, the MLD displays substantial seasonal fluctuations in climatology (contours in Fig. 2a–c). The MLD is generally deep during the local winter season (June–July–August–September, JJAS) south of 10°S. In the NIO, the MLD exhibits two peaks at JJAS and December–January–February–March (DJFM), respectively, with a deeper MLD during DJFM than JJAS north of 10°N.

During the CO_2 ramp-up period (Fig. 2a), the MLD change also shows pronounced seasonal differences. Seasons with deep climatology MLD (larger than 50 m) tend to have a large shoaling trend (i.e., deep-get-shallower), which largely weakens the MLD seasonal cycle in the TIO. Similarly, the MLD deepening trend during the CO_2 ramp-down period also primarily appears during season with deep climatology MLD (Fig. 2b) (i.e., deep-get-deeper). This indicates that CDR actions would largely recover the weakened MLD seasonal cycle induced by the increased atmospheric CO_2. The overall MLD trend displays significant north–south and seasonal differences (Fig. 2c), with a notable deepening trend in DJFM in NIO and a slight shoaling trend in JJAS across both hemispheres. However, the overall shoaling trend south of 10°S displays relatively weak seasonal differences, indicating insignificant changes in seasonal MLD contrast. The results suggest that the seasonal contrast or seasonal cycle of MLD is largely enhanced north of 10°N but may remain nearly unchanged in the south TIO when atmospheric CO_2 is restored.

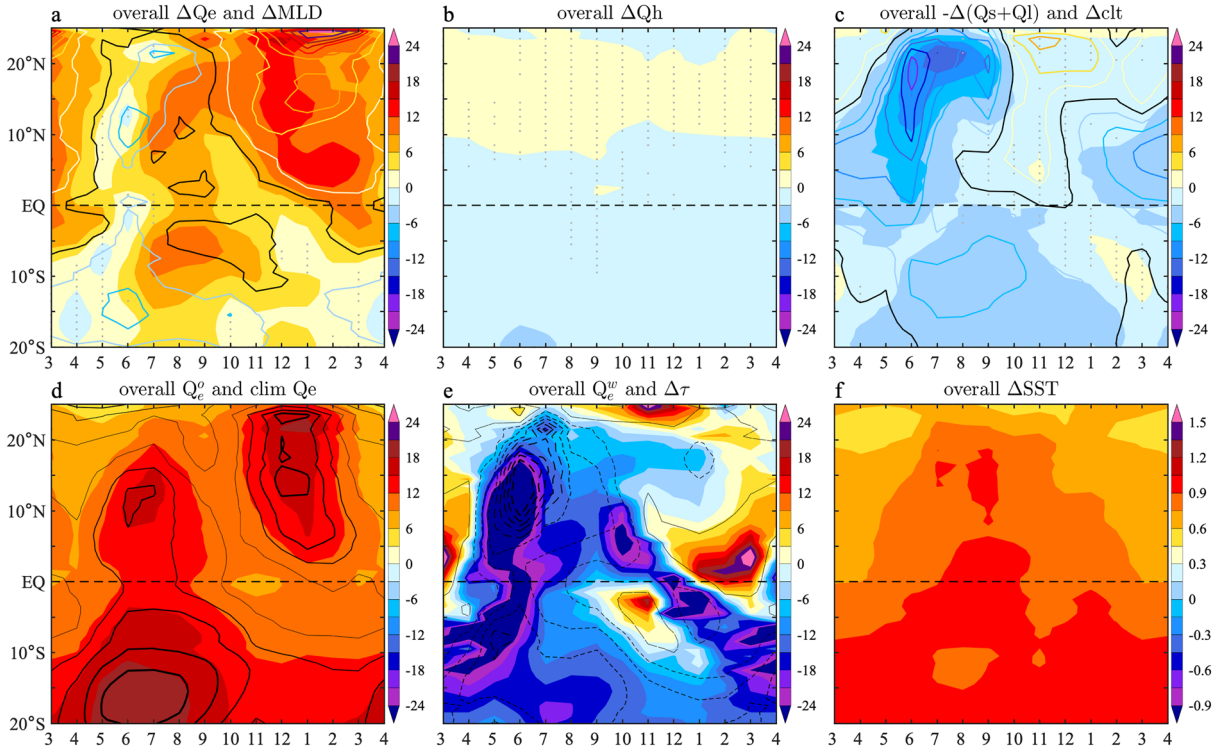

Fig. 3 Seasonal evolution of the zonal–mean overall linear trends during the whole period in Indian Ocean (**a**) MLD (Δ*MLD*, m, contours) and latent heat flux ΔQ_e (W/m^2, shading, positive upward), (**b**) sensible heat flux ΔQ_h (W/m^2, shading, positive upward), (**c**) shortwave and longwave radiative flux $-\Delta(Q_s + Q_l)$ (W/m^2, shading, positive upward) and total cloud cover (Δ*clt*, %, contours), (**d**) Newtonian cooling Q_e^o (W/m^2, shading) and climatology Q_e, (**e**) wind effect in latent heat change Q_e^w (W/m^2, shading) and wind stress ($\Delta\tau$, N/m^2, contours), and (**f**) the SST change between the initial and final 10 years of the whole period. The black thick lines in panel (**a**) indicate the zero contours

Underlying mechanisms of the seasonal differences in MLD responses

Seasonal evolutions of the zonal–mean surface forcing and ocean dynamical contributions further reveal the processes driving the seasonal MLD changes. In the NIO, the overall MLD deepening during DJFM (contours in Fig. 2d–f) is dominated by the prominent surface buoyancy loss from reduced surface net heat flux (i.e., positive $-\Delta BuoyT$, Fig. 2d) rather than freshwater flux (Fig. 2e). Wind forcing plays a negligible role as its changes are weak (Fig. 2f). In contrast, the overall JJAS MLD shoaling is dominated by the reduced Indian summer monsoon winds in the NIO and southeast trade winds in the south TIO, as illustrated by the zero contours in Fig. 2f. Moreover, the weakening of the trade winds is also evident across seasons, leading to a persistent MLD shoaling south of 10°S throughout the year. The effect from Ekman pumping and ocean advection is relatively minor, as their seasonal evolution substantially differ from that of the MLD changes (Fig. 2g, h). Therefore, the seasonal response of surface heat flux and wind forcing primarily explain the seasonal MLD changes in the TIO.

It is interesting that why the surface heat input is largely decreased (positive $-\Delta Q_{net}$) in DJFM but increased (negative $-\Delta Q_{net}$) in JJAS in the NIO. When decomposing the surface net hat flux into different components, it is clear that the increased surface latent heat loss (positive upward, Fig. 3a) is dominant in the NIO, while the contribution from sensible heat changes is negligible (Fig. 3b). The increased surface radiative forcing (shading in Fig. 3c), mainly shortwave (not shown) and resulting from reduced cloud cover (contours in Fig. 3c), also contributes to the increased surface buoyance and hence MLD shoaling in JJAS. We thus further investigate two important components of the latent heat change. The delayed ocean slow response from the deep ocean thermal inertia (Held et al. 2010; Chadwick et al. 2013; Long et al. 2014, 2020) results in an overall SST warming in the Indian Ocean (Fig. 3f) with relatively weak seasonal differences (Fig. 3f). The Newtonian cooling (Q_e^o, positive upward) is thus large over seasons with intense climatology latent heat loss, mainly JJAS and DJFM. However, surface winds (contours in Fig. 3e) slightly weaken in the NIO during DJFM, which cannot suppress the surface warming-induced Newtonian cooling (shading Fig. 3e),

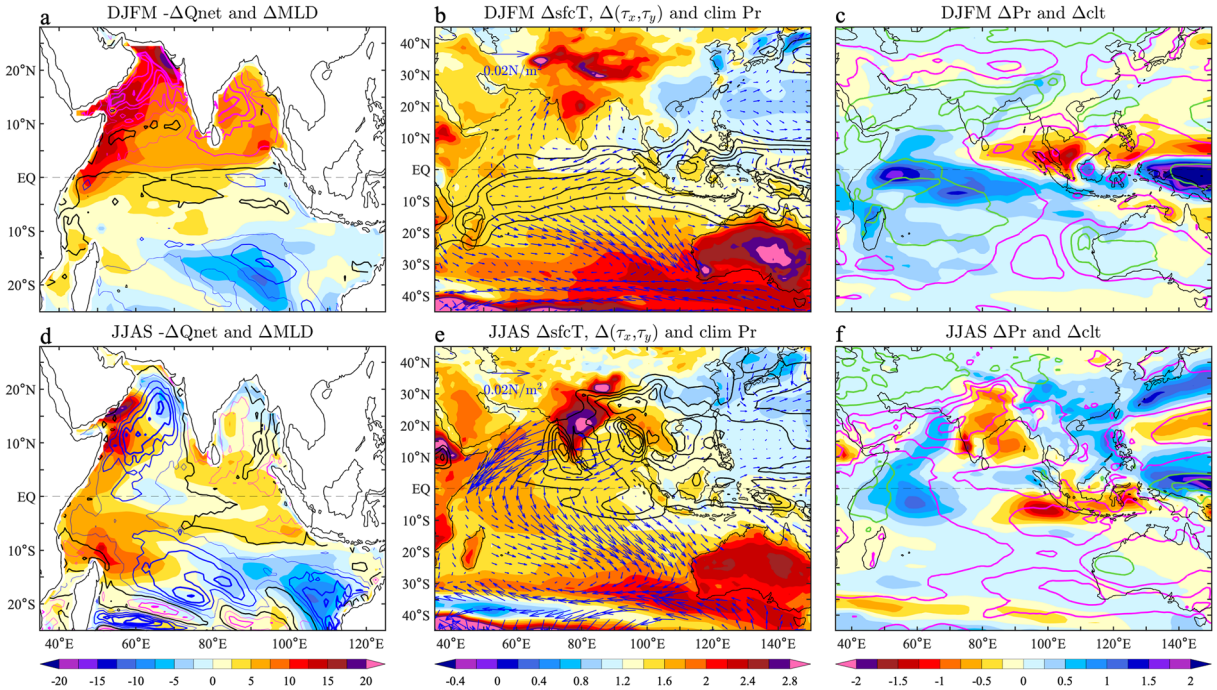

Fig. 4 Spatial patterns of DJFM overall trends during the whole period in (**a**) surface net heat flux ($-\Delta Q_{net}$, shading, positive upward) and MLD (m, contours), (**b**) surface temperature (ΔsfcT), surface wind stress change ($\Delta\tau$, vectors), and climatology precipitation larger than 5 mm/day, and (**c**) precipitation (ΔPr, mm/day, shading) and total cloud cover (Δclt, contours, magenta for decreased cloud and green for increased cloud). Panels (**d**–**f**) are the same as (**a**–**c**) but for JJAS

resulting in substantial latent heat loss residual from the ocean. While the significantly weakened winds during JJAS in the NIO and throughout the year in the south TIO efficiently suppress the latent heat loss through WES feedback, as indicated by large Q_e^w (Fig. 3e), largely mitigating the Newtonian cooling and lead to an overall weak ΔQ_e.

The above results reveals that the reduced wind stress and associated surface warming and heat flux adjustments, especially the latent component, are essential in the overall trends of Indian Ocean MLD after symmetrical CO_2 increase and decrease. To further explore the detailed underlying processes of the MLD changes, we examine the spatial pattern of the overall trends of surface net heat flux, wind stress and associated coupling variables (Fig. 4) in DJFM and JJAS. In DJFM, the broad overall MLD deepening pattern in the NIO (contours in Fig. 4a) is associated with prominent surface heat loss (positive $-Q_{net}$, shading), nearly spatial uniform surface warming but slightly weakened DJFM monsoon (Fig. 4b). The precipitation and clod cover are enhanced in the western Indian Ocean while decreased in the eastern Indian Ocean and Marinetime Continent (Fig. 4c), with relatively large easterly wind anomalies at the equator.

In JJAS, the MLD shoaling in the Arabian Sea (Fig. 4d) accompanies with increased JJAS surface heat (negative $-Q_{net}$, Fig. 4d) around the Indian Subcontinent and pronounced northeasterly wind anomalies (Fig. 4e), indicating weakened JJAS monsoon. The reduced JJAS winds are tightly coupled with reduced (increased) cloud cover and precipitation in the northeastern Indian Ocean (western Indian Ocean) (Fig. 4f), while the surface warming still displays relatively weak spatial variations (Fig. 4e). In compare to the contrast JJAS and DJFM responses in the NIO, there is year-round MLD shoaling south of 10°S. The winds converge from the equatorial ocean to the south, significantly reducing the southeast trade winds.

The weak changes in DJFM winds in the NIO (vectors in Fig. 4c) are to some extent associated with the land–sea thermal contrast change as the Indian Subcontinent warms more than the Indian Ocean when atmospheric CO_2 is restored (Fig. 4c). Moreover, the precipitation changes primarily display large west–east gradients but weak meridional differences (Fig. 4b), accompanied by prominent easterly wind anomalies within 10°S–10°N and minor southerly anomalies in the NIO. This pattern suggests large zonal circulation changes in the equatorial oceans but weak DJFM meridional wind changes in the NIO, possibly due to a zonally distributed Intertropical Convergence Zone (ITCZ) at the equator (black contours in Fig. 4b). It also indicates that the Walker circulation adjustment is important in the DJFM Indian Ocean

response through the Bjerknes feedback (Bjerknes 1969; Liu et al. 2015).

However, the prominent JJAS monsoon weakening seems to be not primarily determined by the land–sea thermal contrast as the Indian Subcontinent still warms more than the Indian Ocean (shading in Fig. 4c, f). Instead, previous studies reveal that the Indian summer monsoon weakening under CDR scenarios may principally result from the moisture–circulation coupling processes (Shaw and Voigt 2015; Li and Ting 2017; Zhang et al. 2024b), which is to some extent similar to the monsoon response to the anthropogenic aerosols (Lau et al. 2006; Wang et al. 2019). This is supported in Fig. 4e, f, which shows that surface winds converge from the Indian Subcontinent and the Bay of Bengal, where precipitation and cloud decrease, into the west Indian Ocean and the equator, where precipitation and cloud increase. It is interesting that the meridional wind changes are prominent and much larger than the zonal winds in JJAS. This phenomenon may be caused by two factors: (1) the ITCZ locates farther north of the equator over the South Asia (black contours in Fig. 4e), in contrast to the DJFM case and (2) the magnitude of the surface meridional winds is much larger in JJAS than DJFM in climatology (Fig. S5) and the spatial pattern of precipitation and wind changes are highly coupled in both seasons following the Gill pattern (Gill 1980). Therefore, the locations of DJFM and JJAS ITCZ may, respectively, favor zonal and meridional wind changes through ocean–atmosphere coupling processes in the overall response to symmetrical CO_2 increase and decrease. However, further in-depth investigation is needed to fully reveal the relative roles of local ocean–atmosphere coupling and surrounding large-scale temperature gradients in driving future Indian monsoon changes (Paik et al. 2024).

Moreover, the persistent northwesterly wind anomalies south of 10°S (Fig. 4b, e) and easterly wind anomalies in the SO across seasons indicate a year-round weakening of the southwest trade winds in the south TIO and westerly in the SO (black and cyan vectors in Fig. S5). This is attributed to the enhanced SO surface warming and is explained by the delayed deep ocean slow response or deeper ocean thermal inertia to external forcing, which preferentially lead to an enhanced SO surface warming when CO_2 decreases (Long et al. 2020; Oh et al. 2024; Zhang et al. 2024b) or hundreds and even thousands of years after the initial fast increase in atmospheric CO_2 (Held et al. 2010; Long et al. 2014; Liu et al. 2024b).

The results reveal the dominant role of atmosphere circulation changes and associated ocean–atmosphere coupling processes in regulating the TIO oceanic environment. We also note that there are substantial model-to-model differences in the seasonal MLD response (Fig. S6). In the NIO, the inter-model differences in the overall MLD trend display positive correlation with those of the wind stress, with a high correlation coefficient of 0.95 and 0.92 between them in DJFM and JJAS, respectively, and the results are similar south of 10°S ($r = 0.94$ and 0.87). This further confirms that the model-projected atmospheric circulation changes primarily determine the MLD response and thus is the key source of improving the projections in Indian Ocean environment changes.

Summary and discussion

The seasonal response of TIO MLD under an idealized scenario with symmetric atmospheric CO_2 increase and decrease has been analyzed to examine the irreversibility of oceanic conditions under CDR actions. The results show that the Indian Ocean basin–mean MLD first shoals as CO_2 increases and subsequently recovers when CO_2 decreases. In both the NIO and south of 10°S, the MLD shoaling (deepening) during the CO_2 ramp-up (ramp-down) period is much larger during the deep MLD season than shallow MLD season, i.e., deep-get-shallower (deep-get-deeper). However, the MLD shoaling trend during CO_2 ramp-up period is not exactly neutralized by the subsequent MLD deepening trend during the CO_2 ramp-down period at regional scale. There is a prominent overall MLD deepening trend in the NIO around the Indian Subcontinent, which primarily appears during DJFM but turns to be an overall shoaling trend during JJAS. This largely amplifies the seasonal MLD contrast, i.e., seasonal cycle amplitude, north of 10°N. Oppositely, the MLD south of 10°S displays an overall shoaling trend but is weak in both magnitude and seasonal variations.

Furthermore, the changes in surface winds and the underlying residual sea surface warming jointly regulate the north–south differences in the overall seasonal MLD changes when atmospheric CO_2 is restored to the preindustrial level. In the NIO, the dominant role of surface heat flux change on the overall DJFM MLD deepening is a compound result of a large Newtonian cooling and a weak wind-induced latent heat change. While the summer MLD shoaling in the NIO is determined by the reduced Indian summer monsoon. Despite an increased surface radiative heat flux associating with cloud and precipitation changes also favors the JJAS MLD shoaling (Fig. 2i), it can further be traced back to the weakened JJAS monsoon (Fig. 3e). In comparison, the prominent trade winds weakening, resulting from the enhanced SO warming, dominates the overall MLD shoaling south of 10°S. In addition, the large residual surface ocean warming at the final state is a result of the delayed ocean slow response due to huge thermal inertia from the deep ocean (Held et al. 2010; Chadwick et al. 2013; Long et al. 2014, 2020; Zhang et al. 2024b) and ocean dynamics

associating with the meridional overturning circulation (Liu et al. 2018; Sun et al. 2022).

The present study highlights that the immediate CDR actions after high carbon emissions would largely recover the CO_2 increase-induced MLD shoaling and resultant seasonal cycle changes over most regions but may still leave irreversible changes. Given that the seasonal evolution of MLD prominently impact the seasonal cycle of SST (Liu et al. 2024a; Shi et al. 2024), marine heatwaves (Amaya et al. 2021; Shi et al. 2022), as well as upper ocean Chlorophyll and nutrients, oxygen and primary production (Kumar et al. 2001), these results can help understanding the model-projected changes in climate and biological systems under potential CDR scenarios in the future (Athira et al. 2025).

Supplementary Information

The online version contains supplementary material available at https://doi.org/10.1186/s40562-025-00383-9.

Supplementary material 1.

Acknowledgements
We acknowledge the International Argo Program providing the Argo datasets. We acknowledge the World Climate Research Programme for coordinating and promoting CMIP6. We also thank the climate modeling groups for producing and making available their model output, the Earth System Grid Federation (ESGF) for archiving the data and providing access.

Author contributions
S.L., Z.G., and C.S. wrote the main manuscript text and prepared all figures. S.L., M.F., X.Q., G.H., and X.C. revised and edited the main text. All authors contributed to the manuscript.

Funding
This work is supported by the Natural Science Foundation of China (42141019, 42076208, 41831175, 41706026), National Key Research and Development Program of China (2017YFA0604600), Natural Science Foundation of Jiangsu Province (BK20211209), Fundamental Research Funds for the Central Universities (B210202135, B210201015).

Availability of data and materials
The BOA Argo data is available from https://argo.ucsd.edu/data/argo-data-products/ and CMIP6 outputs are available from https://esgf-ui.ceda.ac.uk/cog/search/cmip6-ceda/.

Declarations

Competing interests
The authors declare no competing interests.

Author details
[1]Key Laboratory of Marine Hazards Forecasting, Ministry of Natural Resources, Hohai University, Nanjing 210098, China. [2]College of Oceanography, Hohai University, Nanjing 210098, China. [3]CSIRO Environment, Indian Ocean Marine Research Center, Crawley, WA, Australia. [4]Ocean University of China, Qingdao 266100, China. [5]Laoshan Laboratory, Qingdao 266237, China. [6]Center for Monsoon System Research, Institute of Atmospheric Physics, Chinese Academy of Sciences, Beijing 100029, China. [7]State Key Laboratory of Numerical Modeling for Atmospheric Sciences and Geophysical Fluid Dynamics, Institute of Atmospheric Physics, Chinese Academy of Sciences, Beijing 100029, China. [8]National Key Laboratory of Earth System Numerical Modeling and Application, Institute of Atmospheric Physics, Chinese Academy of Sciences, Beijing 100029, China. [9]University of Chinese Academy of Sciences, Beijing 100049, China. [10]Ministry of Natural Resources, The National Marine Environmental Forecasting Center, Beijing 100081, China.

Received: 8 February 2025 Accepted: 15 March 2025
Published online: 03 April 2025

References

Amaya DJ, Alexander MA, Capotondi A, Deser C, Miller AJ (2021) Are long-term changes in mixed layer depth influencing North Pacific marine heatwaves? Bull Am Meteor Soc 102:S59–S66. https://doi.org/10.1175/BAMS-D-20-0111.1

Athira K, Ghoshal PK, Joshi AP, Rose L, Chakraborty K (2025) Understanding future changes of Chlorophyll-a in the Indian Ocean using CMIP6 earth system model simulations. Deep Sea Res Part II Top Stud Oceanogr. https://doi.org/10.1016/j.dsr2.2025.105458

Bjerknes J (1969) Atmospheric teleconnections from the equatorial Pacific. Mon Weather Rev 97:163–172. https://doi.org/10.1175/1520-0493(1969)097%3c0163:ATFTEP%3e2.3.CO;2

Bourgeois T, Goris N, Schwinger J, Tjiputra JF, Heinze C (2022) Stratification constrains future heat and carbon uptake in the Southern Ocean between 30°S and 55°S. Nat Commun 13:340. https://doi.org/10.1038/s41467-022-28074-4

Breitburg D, Levin LA, Oschlies A, Grégoire M, Chavez FP, Conley DJ, Zhang J (2018) Declining oxygen in the global ocean and coastal waters. Science. https://doi.org/10.1126/science.aam7240

Cai R-S, Han Z-Q, Yang Z-X (2020) Impacts and risks of changing ocean on marine ecosystems and dependent communities and related responses. Clim Change Res 16:182–193. https://doi.org/10.3969/j.issn.1673-1719.2020.02.002

Carton JA, Grodsky SA, Liu H (2008) Variability of the oceanic mixed layer, 1960–2004. J Clim 21(5):1029–1047

Chadwick R, Wu P, Good P, Andrews T (2013) Asymmetries in tropical rainfall and circulation patterns in idealised CO_2 removal experiments. Clim Dyn 40:295–316. https://doi.org/10.1007/s00382-012-1287-2

Chen C, Wang G (2015) Role of North Pacific mixed layer in the response of SST annual cycle to global warming. J Clim 28:9451–9458

Cheng L, Abraham J, Trenberth KE, Reagan J, Zhang HM, Storto A, Zhu J (2025) Record high temperatures in the ocean in 2024. Adv Atmos Sci. https://doi.org/10.1007/s00376-025-0001-2

Chu PC, Fan CW (2021) Maximum angle method for determining mixed layer depth from sea glider data. J Oceanogr 67:219–230. https://doi.org/10.1007/s10872-021-00580-7

Elzahaby Y, Schaeffer A, Roughan M et al (2022) Why the mixed layer depth matters when diagnosing marine heatwave drivers using a heat budget approach. Front Clim 4:838017. https://doi.org/10.3389/fclim.2022.838017

Eyring V, Bony S, Meehl GA et al (2016) Overview of the coupled model intercomparison project phase 6 (CMIP6) experimental design and organization. Geosci Model Dev 9:1937–1958. https://doi.org/10.5194/gmd-9-1937-2016

Field CB, Mach KJ (2017) Rightsizing carbon dioxide removal. Science 356:706–707. https://doi.org/10.1126/science.aam9726

Fu W, Randerson JT, Moore JK (2016) Climate change impacts on net primary production (NPP) and export production (EP) regulated by increasing stratification and phytoplankton community structure in the CMIP5 models. Biogeosciences 13:5151–5170. https://doi.org/10.5194/bg-13-5151-2016

Gao Z, Long S-M, Shi J-R et al (2023) Indian Ocean mixed layer depth changes under global warming. Front Clim 5:1112713. https://doi.org/10.3389/fclim.2023.1112713

Gao Z, Zhao S, Liu Q, Long S-M, Sun S (2024) Assessment of the southern ocean sea surface temperature biases in CMIP5 and CMIP6 models. J Ocean Univ China 23(5):1135–1150. https://doi.org/10.1007/s11802-024-5808-5

Gill AE (1980) Some simple solutions for heat-induced tropical circulation. Q J R Meteorol Soc 106(449):447–462. https://doi.org/10.1002/qj.49710644905

Held IM, Winton M, Takahashi K et al (2010) Probing the fast and slow components of global warming by returning abruptly to preindustrial forcing. J Clim 23:2418–2427. https://doi.org/10.1175/2009JCLI3466.1
Jacob SD, Shay LK, Mariano AJ et al (2000) The 3D oceanic mixed layer response to hurricane Gilbert. J Phys Oceanogr 30:1407–1429. https://doi.org/10.1175/1520-0485(2000)030%3c1407:TOMLRT%3e2.0.CO;2
Keller DP, Lenton A, Scott V et al (2018) The carbon dioxide removal model intercomparison project (CDRMIP): rationale and experimental protocol for CMIP6. Geosci Model Dev 11:1133–1160. https://doi.org/10.5194/gmd-11-1133-2018
Kumar SP, Ramaiah N, Gauns M et al (2001) Physical forcing of biological productivity in the Northern Arabian Sea during the Northeast Monsoon. Deep-Sea Res Part II: Top Stud Oceanogr 48:1115–1126. https://doi.org/10.1016/S0967-0645(00)00133-9
Lau KM, Kim MK, Kim KM (2006) Asian summer monsoon anomalies induced by aerosol direct forcing: the role of the Tibetan Plateau. Clim Dyn 26:855–864. https://doi.org/10.1007/s00382-006-0114-z
Li XQ, Ting MF (2017) Understanding the Asian summer monsoon response to greenhouse warming: the relative roles of direct radiative forcing and sea surface temperature change. Clim Dyn 49:2863–2880. https://doi.org/10.1007/s00382-016-3481-4
Li H, Xu F, Zhou W et al (2017) Development of a global gridded Argo data set with Barnes successive corrections. J Geophys Res Oceans 122:866–889. https://doi.org/10.1002/2016JC012285
Li G, Cheng L, Zhu J et al (2020) Increasing ocean stratification over the past half-century. Nat Clim Chang 10:1116–1123. https://doi.org/10.1038/s41558-020-00918-2
Li Z, England MH, Groeskamp S (2023) Recent acceleration in global ocean heat accumulation by mode and intermediate waters. Nat Commun 14:6888. https://doi.org/10.1038/s41467-023-42468-z
Liu Q, Lu Y (2016) Role of horizontal density advection in seasonal deepening of the mixed layer in the subtropical Southeast Pacific. Adv Atmos Sci 33(4):442–451. https://doi.org/10.1007/s00376-015-5111-x
Liu W, Lu J, Xie S-P (2015) Understanding the Indian ocean response to double CO_2 forcing in a coupled model. Ocean Dyn 65:1037–1046. https://doi.org/10.1007/s10236-015-0854-6
Liu W, Lu J, Xie S-P, Fedorov A (2018) Southern ocean heat uptake, redistribution, and storage in a warming climate: The role of meridional overturning circulation. J Clim 31:4727–4743
Liu F, Song F, Luo Y (2024a) Human-induced intensified seasonal cycle of sea surface temperature. Nat Commun 15:3948. https://doi.org/10.1038/s41467-024-35793-w
Liu W, Li S, Li C, Rugenstein M, Thomas AP (2024b) Contrasting fast and slow intertropical convergence zone migrations linked to delayed Southern ocean warming. Nat Clim Chang 14:732–739. https://doi.org/10.1038/s41558-024-02034-x
Long S-M, Xie S-P, Zheng X-T et al (2014) Fast and slow responses to global warming: Sea surface temperature and precipitation patterns. J Clim 27:285–299. https://doi.org/10.1175/JCLI-D-13-00297.1
Long S-M, Xie S-P, Du Y et al (2020) Effects of ocean slow response under low warming targets. J Clim 33:477–496. https://doi.org/10.1175/JCLI-D-19-0346.1
Long S-M, Zhao S, Gao Z, Sun S, Shi J-R, Ying J et al (2024) Weakened seasonality of the ocean surface mixed layer depth in the Southern Indian Ocean during 1980–2019. Geophys Res Lett. https://doi.org/10.1029/2023GL107644
Oh JH, Kug JS, An SI, Jin FF, McPhaden MJ, Shin J (2024) Emergent climate change patterns originating from deep ocean warming in climate mitigation scenarios. Nat Clim Chang. https://doi.org/10.1038/s41558-024-01806-7
Paik S, Kim D, An SI et al (2024) Exploring causes of distinct regional and subseasonal Indian summer monsoon precipitation responses to CO_2 removal. npj Clim Atmos Sci. https://doi.org/10.1038/s41612-024-00426-2
Pang S, Wang X, Vialard J (2024) How well do CMIP6 models simulate salinity barrier layers in the North Indian Ocean? J Clim 37(1):289–308. https://doi.org/10.1175/JCLI-D-23-0366.1
Peng S, Wang Q (2024) Fast enhancement of the stratification in the Indian Ocean over the past 20 years. J Clim 37:2231–2245. https://doi.org/10.1175/JCLI-D-23-0601.1
Roch M, Brandt P, Schmidtko S (2023) Recent large-scale mixed layer and vertical stratification maxima changes. Front Mar Sci 10:1277316
Sallée JB, Pellichero V, Akhoudas C et al (2021) Summertime increases in upper-ocean stratification and mixed-layer depth. Nature 591:592–598. https://doi.org/10.1038/s41586-021-03303-x
Sanderson BM, Xu YY, Tebaldi C, Wehner M, O'Neill B, Jahn A et al (2017) Community climate simulations to assess avoided impacts in 1.5 and 2°C futures. Earth Syst Dynam 8:827–847. https://doi.org/10.5194/esd-8-827-2017
Shaw TA, Voigt A (2015) Tug of war on summertime circulation between radiative forcing and sea surface warming. Nat Geosci 8:560–565. https://doi.org/10.1038/ngeo2449
Shi J, Tang C, Liu Q et al (2022) Role of mixed layer depth in the location and development of the Northeast Pacific warm blobs. Geophys Res Lett. https://doi.org/10.1029/2022GL098849
Shi JR, Santer BD, Kwon YO, Wijffels SE (2024) The emerging human influence on the seasonal cycle of sea surface temperature. Nat Clim Chang 14:364–372. https://doi.org/10.1038/s41558-024-01840-5
Somavilla R, Gonzalez-Pola C, Fernandez-Diaz J (2017) The warmer the ocean surface, the shallower the mixed layer. How much of this is true? J Geophys Res: Oceans 122:7698–7716. https://doi.org/10.1002/2017JC013125
Sun S, Thompson A, Xie S-P, Long S-M (2022) Indo-Pacific warming induced by a weakening of the Atlantic meridional overturning circulation. J Clim 35(2):587–604. https://doi.org/10.1175/JCLI-D-21-0346.1
Wang H, Xie SP, Kosaka Y, Liu Q, Du Y (2019) Dynamics of Asian summer monsoon response to anthropogenic aerosol forcing. J Clim 32(3):843–858. https://doi.org/10.1175/JCLI-D-18-0386.1
Wu P, Wood R, Ridley J, Lowe J (2010) Temporary acceleration of the hydrological cycle in response to a CO_2 rampdown. Geophys Res Lett 37:L12705. https://doi.org/10.1029/2010GL043730
Xie S-P, Philander SGH (1994) A coupled ocean-atmosphere model of relevance to the ITCZ in the eastern Pacific. Tellus A 46(4):340–350. https://doi.org/10.1034/j.1600-0870.1994.t01-1-00001.x
Xie S-P, Deser C, Vecchi GA, Ma J, Teng H, Wittenberg AT (2010) Global warming pattern formation: Sea surface temperature and rainfall. J Clim 23(4):966–986. https://doi.org/10.1175/2009JCLI3329.1
Yeh S-W, Yim BY, Noh Y et al (2009) Changes in mixed layer depth under climate change projections in two CGCMs. Clim Dyn 33:199–213. https://doi.org/10.1007/s00382-009-0530-4
Zhang S, Qu X, Huang G et al (2023) Asymmetric response of South Asian summer monsoon rainfall in a carbon dioxide removal scenario. npj Clim Atmos Sci. https://doi.org/10.1038/s41612-023-00294-7
Zhang Y, Chen C, Hu S, Wang G, McMonigal K, Larson SM (2024) Summer westerly wind intensification weakens Southern Ocean seasonal cycle under global warming. Geophys Res Lett. https://doi.org/10.1029/2024GL109715
Zhang S, Qu X, Huang G, Hu P, Zhou S, Wu L (2024) Delayed onset of Indian summer monsoon in response to CO_2 removal. Earth's Future. https://doi.org/10.1029/2023EF004039
Zhou S, Huang P, Xie S-P, Huang G, Wang L (2022) Varying contributions of fast and slow responses cause asymmetric tropical rainfall change between CO_2 ramp-up and ramp-down. Sci Bull 67:1702–1711. https://doi.org/10.1016/j.scib.2022.06.017

Publisher's Note